Gradient Droplet Arrays by Acceleration Mode Dip Coating

Nikolaj K. Mandsberg,* Anna V. Shneidman, Kaare H. Jensen, Rafael Taboryski, Line H. Nielsen, Joanna Aizenberg, and Anja Boisen

Droplet microarray technology is of great interest in biology and chemistry as it allows for signiocant reactant savings and massive parallelization of experiments. Upon scaling down the footprint of each droplet in an array, it becomes increasingly challenging to produce the array drop by drop. Therefore, techniques for parallelized droplet production are developed, e.g., dip Loating of biphilic substrates. However, it is in general difficult to tailor the characteristics of individual droplets, such as size and content, without updating the substrate. Here, the method of dip coating of uniformly pat□ terned biphilic substrates in solcalled □acceleration □mode □ to produce droplet arrays featuring gradients in droplet height for 0xed droplet footprint is devel0 oped. The results herein present this method applied to produce drops with base diameters varying over orders of magnitude, from as high as 6 mm to as small as 50 μm; importantly, the experimentally measured power law Idepend I ency of volume on capillary humber matches analytical theory for droplet formation on heterogenous substrates though the precise quantitative values likely differ due to 2D substrate patterning. Gradient characteristics, including average droplet volume, steepness of the gradient, and its monotonicity, can all be tuned by changing the diptoating parameters, thus providing a robust method for high@hroughput screening applications and experiments.

N. K. Mandsberg, L. H. Nielsen, A. Boisen The Danish National Research Foundation and Villum Foundation

Center for Intelligent Drug Delivery and Sensing Using Microcontainers and Nanomechanics (IDUN)

Department of Health Technology

Technical University of Denmark

I rsteds Plads, Kgs. Lyngby DKI2800, Denmark

Elmail: nikoma@dtu.dk

A. V. Shneidman, J. Aizenberg

John A. Paulson School of Engineering and Applied Sciences

Harvard University

Cambridge, MA 02138, USA

K. H. Jensen

Department of Physics

Technical University of Denmark

Kgs. Lyngby DKI2800, Denmark

R. Taboryski

DTU Nanolab

National Centre for Nano Fabrication and Characterization

Technical University of Denmark

Kgs. Lyngby DKI2800, Denmark



© 2022 The Authors. Advanced Materials Interfaces published by Wiley VCH GmbH. This is an open access article under the terms of the Crea tive Commons Attribution License, which permits use, distribution and reproduction in any medium, provided the original work is properly cited.

DOI: 10.1002/admi.202200667

1. Introduction

Parallelization of experiments is a pow□ erful method to rapidly acquire scien□ tific evidence, especially important for multiparameter studies. Digital droplet array technologies have become prevalent in chemistry and biochemistry, allowing for experiments to be simultaneously con□ ducted and interrogated within a large number of droplets, each of which func□ tions as an individual microreactor.[104] However, standard techniques for one step formation of droplet arrays□ such as dip□ coating of biphilic substrates□ do not allow for array formation with control over the individual droplets (usually, all are nearly identical in size).^[5] The possibility to pro□ duce dissimilar droplets within an array, e.g., varying in size or content, would allow fast formation of microarrays for screening applications. This could be useful for com□ binatorial chemistry and rapid data collec□ tion for dose□response curves.

Variations in droplet volumes along a substrate have been obtained by varying the size of the hydro□ philic islands on the substrate prepared for dip�aoating, [6□0] but the ability to adaptively tune droplet sizes for a fixed substrate has, to our knowledge, not yet been evaluated. In the case of films, however, researchers achieved continuous films with thick□ ness gradients by performing the dip�aoating[11] or flow�aoating[12] methods in acceleration□node, i.e., accelerating the substrate during withdrawal rather than the typical constant linear velocity.

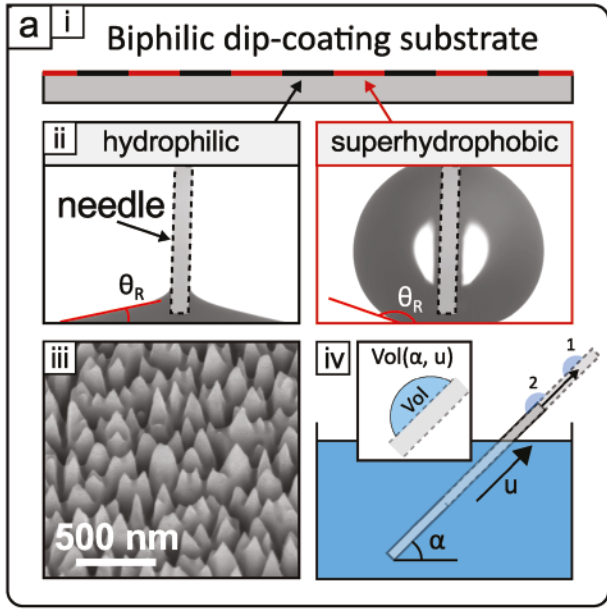
Here, we combine the parallel production of droplet arrays on biphilic substrates, consisting of hydrophilic spots in a hydro□ phobic matrix, with acceleration⊡ mode dip acting to produce height gradients across droplet arrays with fixed droplet base diameters. We show that the method of acceleration mode dip coating for gradient array creation is applicable across two orders of magnitude in droplet base diameters and is expected to extend even further, as well as beyond water droplets demonstrated here.

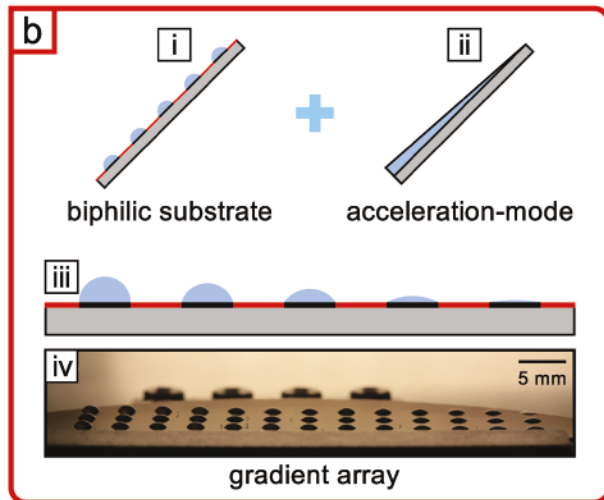
2. Results

2.1. Dip[Coating of Biphilic Substrates to Produce Droplet Arrays

DipEb ating of a biphilic substrate is a standard approach to pro duce droplet arrays. In general, a biphilic substrate is immersed and subsequently withdrawn from a liquid reservoir. [13] As

87359, 2022, 22, Downloaded from https://onlinelibrary.wiley.com/doi/10.1002/admi.202200667, Wiley Online Library on [07/11/2022]. See the Terms and Conditions (https://onlinelibrary.wiley.com/terms-and-conditions) on Wiley Online Library for rules of use; OA articles are governed by the applicable Creative Commons





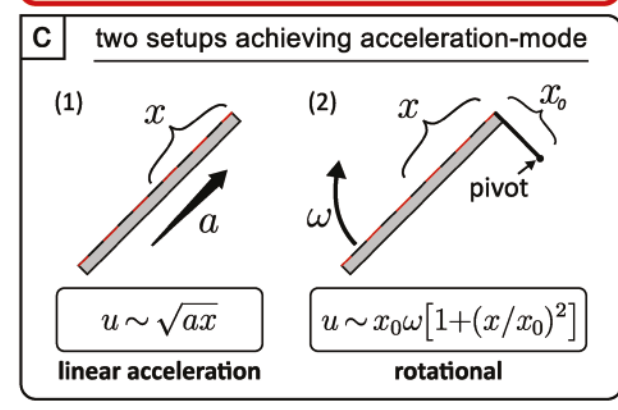


Figure 1. Gradient droplet arrays formed on biphilic substrates by acceleration[mode dip[boating. a) Overview of the dip[boating process to produce droplet arrays. i) The biphilic substrate is shown schemati[] cally, ii) with the receding contact angle, θ_{R} , measured on the distinct regions using the needle method with inflation/deflation protocol. iii) The SEM micrograph shows the nanostructuration on the substrate that enhances the wetting contrast. iv) The dipleoating process is

shown schematically in Figure 1a□v, the technique entails with□ drawing the substrate from a liquid reservoir at an angle, α , and withdrawal speed, u. Because dipto ating is typically fully automated, it offers precise control over several parameters, such as withdrawal speed and angle between substrate and res□ ervoir meniscus, which for millimeter sized droplets have both been shown to affect the volume of all droplets in the array.[10] While decreasing the dipco ating angle (with respect to hori□ zontal) increased the droplet size, the withdrawal speed had a nonmonotonic relationship with size. In the low peed regime, droplet volume increased with speed, while it decreased in the high peed regime where droplet heights are restricted by the viscous boundary layer.[14]

2.2. Chemically and Physically Functionalized Substrates

2.2.1. Substrate Fabrication

The biphilic substrates employed here consisted of regularly spaced identical circular hydrophilic spots in a hydrophobic matrix, with spot diameters ranging from 50 m to 6 mm (Figure 1a□ and Figure S1, Supporting Information). A com□ bination of reactive ion etching (RIE), photolithography, and chemical functionalization of a silicon wafer was used to create the substrate patterning. An initial RIE step was employed to achieve nanoscale roughness across the entire surface in order to enhance the chemically induced wettability contrast, which was assessed with a sessile droplet method, as shown in Figure 1a□i.^[15] The chemical pattern was defined using photo□ lithography, whereby regions masked by photoresist remained hydrophilic, while hydrophobic regions were achieved on the unmasked regions using a perfluorodecyltrichlorosilane (FDTS) coating deposited by molecular vapor deposition. The nano□ rough surface was observed with scanning electron micros□ copy (SEM), revealing a random forest of cone is ke structures, with an average base diameter of (160 \pm 10) nm (calculated as the square root of the average area per cone, using 62 cones, and Poisson counting error) and an average opening angle of (26 ± 7) (Figure 1a□ii). Further details of the substrate fabrica□ tion and characterization are provided in the Experimental Sec□ tion and Section S1.1 in the Supporting Information.

2.2.2. Droplet Formation Criteria and Substrate Wetting Characterization

When dipEb ating biphilic substrates, separate droplets are formed on the hydrophilic spots as the reservoir water recedes

schematically depicted; α , u, and Vol are the withdrawal angle, speed, and resulting droplet volume, respectively. b) Conceptual drawing showing how the combination of i) a biphilic substrate for droplet array creation combined with ii) the ability to produce thickness gradient by dip@oating in acceleration[mode can lead to iii) a gradient droplet array. iv) Photo[] graph of a gradient droplet array produced in this way. c) Schematics of two different realizations of acceleration[mode dip[boating: (1) constant linear acceleration and (2) rotational dipleoating, where the withdrawal speed u varies with droplet location x as indicated. (1) a is the acceleration and (2) ω is the angular velocity at the hinge/pivot.



www.advmatinterfaces.de

Table 1. Wetting characteristics of biphilic substrates.

	Hydrophilic region (SiO ₂)		Hydrophilic region (FDTS)	
	mean	std. dev.	mean	std. dev.
^{a)} Advancing contact angle []	111	3	169	2
^{a)} Receding contact angle []	9	3	161	3
^{b)} Contact angle hysteresis []	102	4	8	4

a)The mean and standard deviations for the advancing and receding contact angles are obtained from three repetitions of the measurement on the same substrate, i.e., a new drop is inflated/deflated on the same substrate but at a different local tion; b)The contact angle hysteresis standard deviation is calculated using error propagation under the assumption of independent variables.

from the substrate during withdrawal. Consequently, to entrain droplets, the hydrophilic spots must pin the water while the surrounding superhydrophobic matrix preferably exhibits low contact angle hysteresis (CAH) in order to shed the water easily, as the adhesion force increases with CAH as described by the Furmidge equation. The nanoroughness used in this work exhibits such strong pinning that the advancing contact angle was larger than 90 on native silicon oxide (i.e., within the hydrophilic spots). This extreme droplet pinning and high advancing contact angle are similar to those observed on rose petals. Meanwhile, the receding contact angle was meas ured to be (9 \pm 3) within the hydrophilic spots on the substrate and the CAH to be (8 \pm 4) in the hydrophobic regions. All advancing/receding contact angles and the CAH for the distinct regions are summarized in Table 1.

2.2.3. Substrate Robustness to Various Treatments

The substrate was subject to acidic, basic, and thermal treat \square ments in order to test the durability of the patterning. We found that droplet arrays continued to successfully form on substrates that had been submerged for 1 week in an aqueous environment of either pH = 0.3 or pH = 11.9 (Figure S12, Sup \square porting Information). The FDTS coating also exhibited great thermal stability, withstanding 300 C for (8 \pm 2) h, in line with published results, [22] which further increases the versatility of the droplet array platform (see Section S3.2 in the Supporting Information for test details).

2.2.4. Producing Gradient Droplet Arrays

As the withdrawal velocity affects the entrained droplet height, arrays featuring drops with fixed footprints and a gradient in heights were achieved by accelerating the biphilic substrate during extraction from the liquid reservoir. The concept is schematically presented in Figure 1b, where the biphilic substrate is necessary for the production of droplet arrays and the nonuniform withdrawal speed is key to generating droplets of different heights on a regular array of identical hydrophilic spots. The photograph in Figure 1b depicts a typical gradient droplet array prepared in this way.

Two different setups were built to vary the velocity of the substrate as it emerged from the reservoir, with details pro□ vided in Sections S2.1 and S2.4 in the Supporting Information.

Whether to use linear (Figure 1c, left) or rotational (Figure 1c, right) dipco ating was determined by the size of the hydro□ philic spots on the substrate. For small (≤1 mm diameter) hydrophilic spots on the substrate, we used linear acceleration dipco ating, in which the substrate was withdrawn from the reservoir at a fixed angle but progressively increasing speed (Figure 1c, left). Rotational dipco ating, in which the sub□ strate was rotated out of the reservoir (Figure 1c, right), was employed for substrates featuring larger hydrophilic footprints, as this setup takes advantage of both the speed and the angular dependency, thereby enabling steeper volume gradients and thus larger height ranges. It is noteworthy that the rotational setup is mostly applicable for larger droplet arrays as the shift in location x throughout the array should be significant com pared to the optional offset from the rotational axis, x_0 (indi cated on Figure 2a \square), to create noticeable gradients (x_0 was on the mm to cmccale due to dimensional constraints of LEGO bricks (LEGO, Billund, Denmark), which was used for building the rotational dipEb ating setup). In the case of constant linear acceleration, a, the withdrawal speed scales with the square root of traveled distance, $u \sim \sqrt{ax}$. For rotational extraction at a con stant angular velocity, ω , defined at the hinge/pivot (the axis of rotation), the withdrawal speed for a droplet at position x (the projected distance from the hinge) is: $u(x) = x_0 \omega [1 + (x/x_0)^2]$. We note that near the $x_0 = 0$ limit, this expression tends to infinity and is not valid.

2.3. Droplet Imaging and Characterization

Three different imaging techniques were employed to either 1) visualize the droplet formation process in realDime and inform theoretical analysis or 2) characterize the resulting droplet arrays. Timela pse imaging of the substrate as it was withdrawn from the reservoir allowed us to gain mechanistic understanding, as described in Section 2.3.1 and illustrated in Figure 2a. We extracted the local withdrawal speed to calculate the capillary number (data and model provided in Section S2.3, Supporting Information), which was then employed to com□ pare with theory, as discussed in Section 3. To characterize the resulting droplet arrays, we measured the heights of the drop□ lets using one of two experimental methods, depending on the droplet size: sideview imaging was sufficient for 1D arrays of larger droplets, while micronsize droplets and 2D arrays required a more nuanced topview imaging technique, both of which are discussed below (Section 2.3.2 and Figure 2b,c).

2.3.1. Visualizing the Droplet Formation Process

The droplet formation process was visualized using time□apse imaging with the camera positioned directly above the sub□ strate where the substrate exits the reservoir (Figure 2a□). The resulting camera view is shown schematically in Figure 2a□it to clarify the photographs in Figure 2a□it. When submerged, the superhydrophobic regions of the substrate appeared sil□ very due to the thin layer of air (plastron) that surrounds it.^[23] This indicates that the liquid is in the Cassie□Baxter state (air filling the surface nanostructuration under the drop), which

18739, 2022, 22, Down added from https://onlinelibrary.wiley.com/doi/10.1002/admi.202200667, Wiley Online Library on [07/11/2022]. See the Terms and Conditions (https://onlinelibrary.wiley.com/terms-and-conditions) on Wiley Online Library for rules of use; OA articles are governed by the applicable Creative Commons

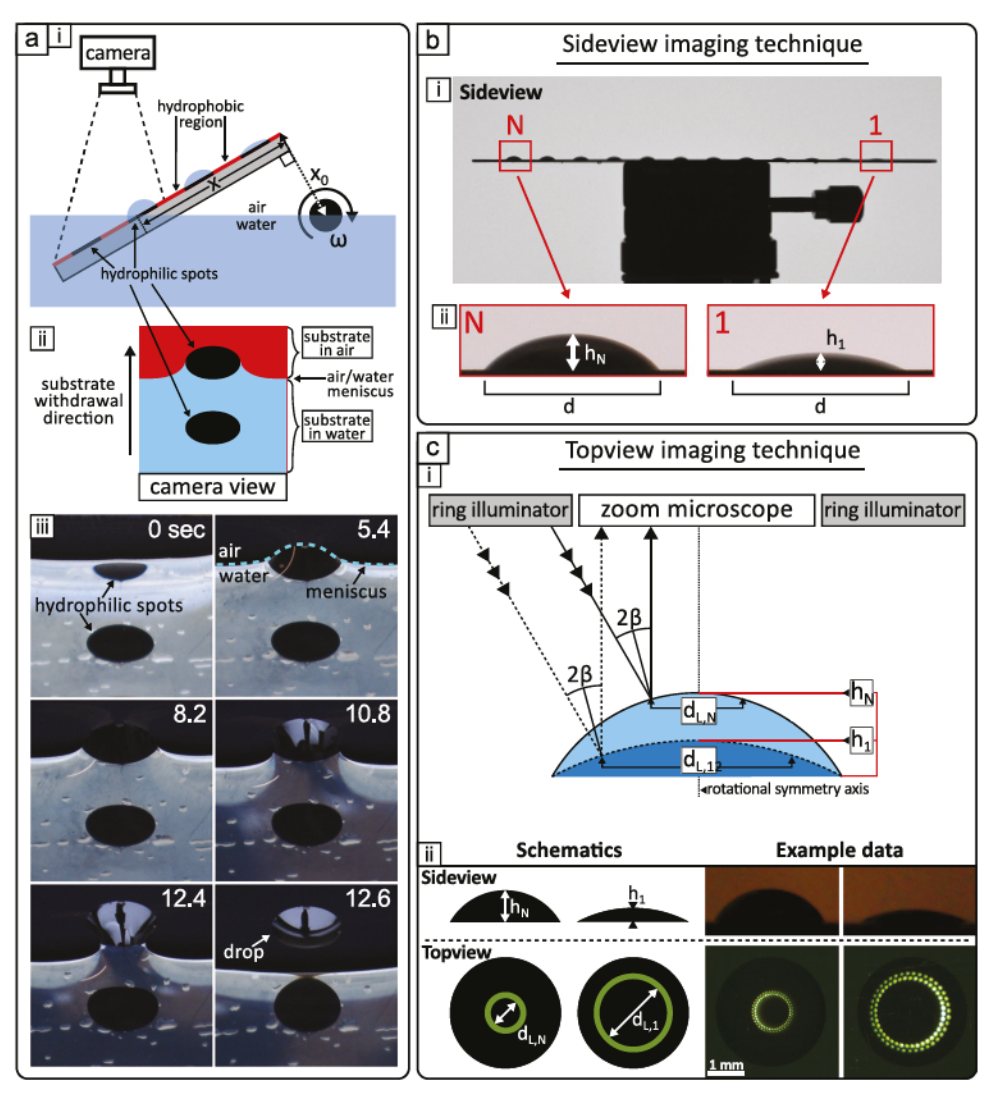


Figure 2. Imaging systems to visualize droplet formation and determine their heights. a) Time lapse imaging of droplet formation process. i) Schematic of the rotational dip lacoting setup. The camera is positioned directly above the location of the air larger trinterface so that droplets can be visualized as they emerge from the reservoir. ii) Schematic of the camera laview. iii) Still images from a time lapse recording of droplet formation (5 mm base diam leter). b) Side laview imaging to determine the heights for millimeter lazed droplets. i) Photograph of gradient droplet array on a stage. ii) Zoom lin on the largest (N) and smallest (1) droplets with h_N , h_1 indicating the measured heights (d = 3 mm; N = 12 here). c) Top laview imaging technique employed to determine the heights of micrometer lazed droplets. i) Schematic showing how the light from a ring illuminator is reflected in two droplets (dark blue droplet has a smaller height h_1 than the light blue droplet with height h_N , leading to a larger reflected diameter for the smaller drop: $d_{L,1} > d_{L,N}$. ii) Schematics (left) and example data (right) showing that droplets with smaller height result in larger reflected diameters; here the droplet footprint diameter was 3 mm.

is generally associated with lower adhesion and CAH than the Wenzel state (liquid fling the nanostructuration). Mean□ while, the hydrophilic spots appeared super black, [24] which is caused by a combination of antireflective and absorbing prop□ erties of the nanotextured substrate combined with the liquid being in the Wenzel state. The part of the substrate extracted from the reservoir appeared black as well on the camera, again due to the antireflective properties of the nanostructuration on the absorbing silicon substrate. Deformation of the liquid meniscus as one hydrophilic region (black circle) emerged from the reservoir can be observed in the still frames acquired with timeta pse imaging. The speed experienced by the individual droplet as it separated from the reservoir, i.e., the withdrawal

speed (Figure S6, Supporting Information), was approximated as the droplet array period (two times the droplet base diam eter) divided by the time difference between extraction of the current droplet and its predecessor. The speed was further used to determine the capillary number for each withdrawn droplet (used in Section 3.2).

2.3.2. Extracting Droplet Heights

Since the droplet footprints are fixed, droplet height is a sufficient descriptor for droplet size. Two different strategies were used to characterize droplet heights. For 1D arrays of www.advancedsciencenews.com

MATERIALS INTERFACES

www.advmatinterfaces.de

millimetersized droplets, the heights were relatively straight□ forward to extract using a sideview imaging setup (Figure 2b). Here, the coated substrate was placed on a level stage imme□ diately following completion of the dipEb ating procedure and imaged from the side at a resolution of 15 m pixel-1. The height was determined using a custom or itten MATLAB script to 1) detect the substrate and calculate its tilt angle, 2) align the substrate to horizontal via image rotation, 3) crop the image, 4) identify the droplets and their positions, and, finally, 5) determine the heights of the droplets using a builtin standard deviation Her (see Figure S4 in the Supporting Infor□ mation for details of the height analysis procedure, including a visualization). We note that in our experiment, we had a detection limit of ≈0.2 mm for resolving the droplet heights, determined by the observed discrepancy between the computer□ aided image analysis and visual inspection of the images.

Side Diew imaging was not an option for the 2D arrays of smaller droplets due to limitations of optical resolution, shad owing effects, and evaporation. Thus, we developed a top Diew imaging technique to simultaneously interrogate the entire 2D array, based on a method used by Campbell, Allain, and Langmuir for single droplet characterization. [25027] In our case, a ring haped light source illuminated the array from above (Figure 2ct) and droplet heights were calculated from the diam eter of the reflection using Equation (1) (see Figures S&S 11 in the Supporting Information for further details on the conversion, analysis procedure, and data with additional sizes)

$$h = \frac{(d_{\rm L}/d)}{2\sin\beta} \left(1 - \sqrt{1 - (d_{\rm L}/d)^{-2}\sin^2\beta} \right) d \tag{1}$$

Equation (1) is valid for droplet contact angles, θ , from β to 90 (because $d_1/d \in [\sin \beta, 1]$), where β is an experimentally determined angle.

Figure 2c provides schematics and example data to illus□ trate the counterintuitive coupling between droplet height, h, and ring reflection diameter, d_1 , where larger d_1 corresponds to smaller h. Because the droplet arrays in all investigated cases were much smaller (≈0.5 cm circumscribed circle radius) than the distance to both the light source (≈9 cm) and the micro□ scope objective (≈6 cm), it was assumed that the reflection was rotationally symmetric throughout the whole array and that the relationship between individual droplet height and reflection diameter did not depend on droplet base diameter. Consequently, larger droplets were used to calibrate the setup; footprint diameters of 2 and 3 mm were chosen to not signifi□ cantly exceed the capillary length, which for water is 2.7 mm, such that they can be approximated as spherical caps (see Section S2.4, Supporting Information). The imaging resolu□ tion here was 6.2 m pixel-1 for arrays with diameters 1000 and 250 m, and 2.3 m pixel⁻¹ for arrays with diameter d = 50 m.

2.4. Resulting Gradient Arrays

As mentioned above, 1D gradient arrays consisting of millim eterslized droplets were created using rotational dipto ating, while 2D arrays of micrometers ized droplets were produced using linear acceleration to de dipto ating. The dependence of

the droplet size on various parameters related to the dynamics and geometry of the setups was investigated.

2.4.1. Gradients for 1D Arrays of Millimeter-Sized Droplets using Rotational Dip-Coating

Rotational dipco ating enables steeper gradients in droplet heights across the substrate, due to variation in both speed and angle, compared to those achievable by linear accel eration. Droplet heights were determined using sideliew imaging and the dependence of height on angular velocity was determined by extracting biphilic substrates at different ω, Figure 3a (see Figures S4 and S5 in the Supporting Infor□ mation for analysis details and additional data, respectively). Angular speeds between 0.58 and 78 s⁻¹ were chosen as these were the minimum and maximum achievable given the gears employed in the setup and the power that could be applied to the motor. We notice that for the largest angular velocity (78 s⁻¹, neon green line), the droplet height first increased and then decreased upon moving away from the hinge due to a transition into the high peed regime (the transition from the lows peed to the highs peed occurs approximately at 16 cm s⁻¹ when the Froude number, effectively the ratio between flow inertia and gravity, is unity).[14] The withdrawal speed remained in the lowspeed regime for all other tested angular velocities, showing an expected increase in droplet height with increasing ω . Likewise, for fixed ω , height increased monotonically for droplets further from the hinge as the extraction speed pro□ gressively increased. Here, we produced droplets with contact angles up to ≈45, but a larger contact angle should be possible to achieve, as we have previously demonstrated the creation of millimetersized droplets (5 and 7 mm in droplet base diam□ eter) with contact angles above 60 using nonacceleration mode dipco ating.[10]

2.4.2. Gradients for 2D Arrays of Micrometer-Sized Droplets using Linear Acceleration Dip-Coating

The biphilic substrates were rotated 45 relative to the reservoir surface normal and were extracted vertically (such that the gra□ dient in droplet heights was along the diagonal of the substrate; see Figure S7, Supporting Information). The method was shown to apply to a large range of hydrophilic spot sizes on the surface (here demonstrated from 50 to 1000 m). The arrays were visualized using the ring illumination method described in Section 2.2.2. Figure 3b□ (top left) schematically depicts the (counterintuitive) correlation between droplet height and ring reflection diameter. The photographs in Figure 3b□ show the ring reflections from droplet arrays produced using three dif□ ferent biphilic substrates, featuring hydrophilic spot diameters of 1000, 250, and 50 m, labeled on the top left of each array (similar images for base diameters of 100 and 500 m are pro□ vided in Figure S11, Supporting Information).

Figure 3bDi shows the dependence of droplet height on droplet position (measured in millimeters from the droplet that first emerged from the reservoir) along the diagonal white arrows in Figure 3bD. The droplet heights were calculated from

1873.92, 2022, 22, Downadded from https://onlinelibrary.wiley.com/doi/10.1002/admi.202200667, Wiley Online Library on [07/11/2022]. See the Terms and Conditions (https://onlinelibrary.wiley.com/terms-and-conditions) on Wiley Online Library for rules of use; OA articles are governed by the applicable Creative Commons

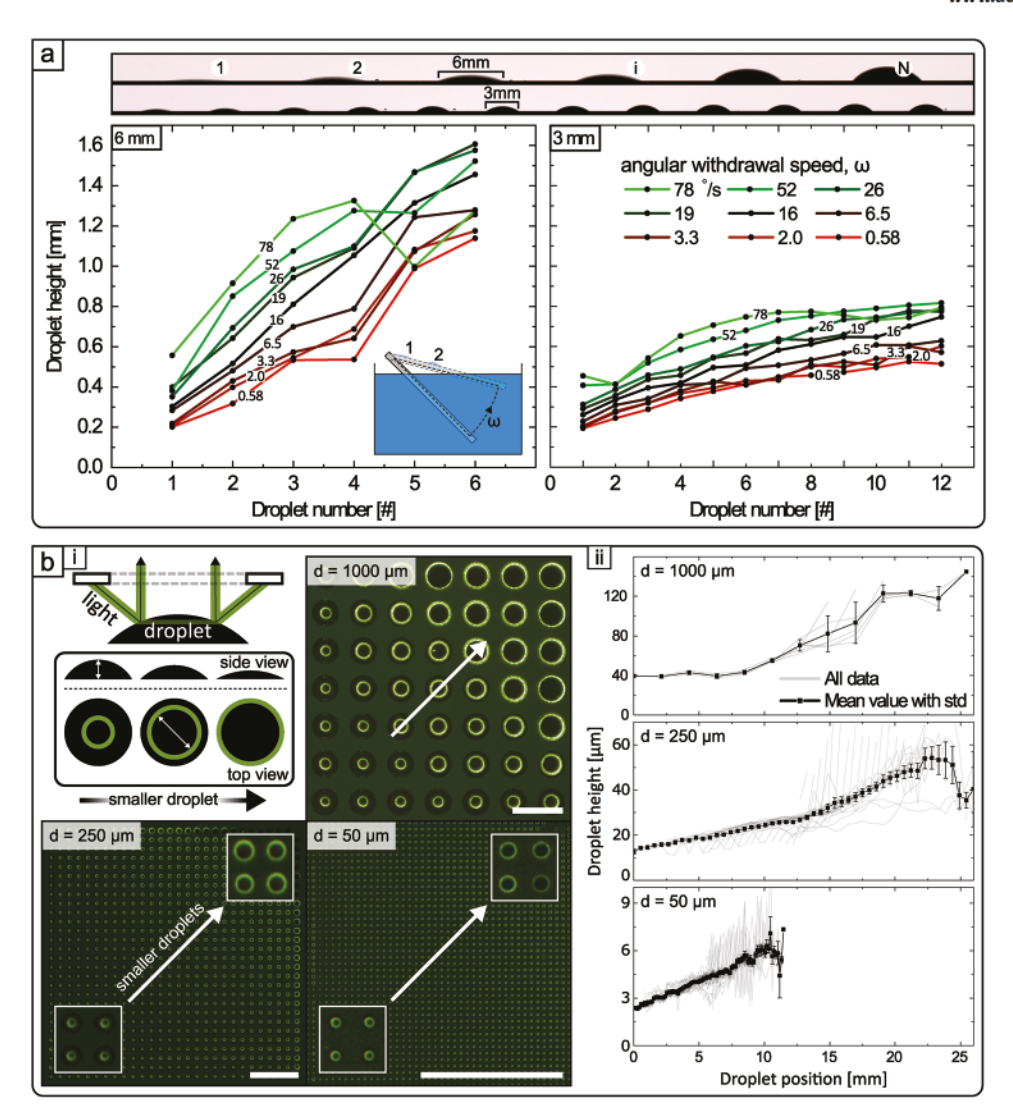


Figure 3. Formation of gradients droplet arrays across length scales. a) 1D arrays of droplets produced by rotational diplcoating (bottomleft inset illustrates the process) for two different substrates with drop base diameters of 6 and 3 mm (sidelbiew photographs at the top show drop arrays for angular velocity $\omega = 3.3~\text{s}^{-1}$ at the hinge). The distance between neighboring droplets in each array equals the diameter of the hydrophilic spots. Plots show the effects of varying the angular velocity on the droplet height, average for n = 5. b) 2D microdroplet arrays produced using acceleration[Imode linear diplcoating of a substrate in the direction of the array diagonal. Droplet diameters of d = 1000, 250, and 50 m are presented with droplto[drop distances of 400, 125, and 50 m, respectively. i) Droplet heights were obtained from the diameter of the reflection of the ring illuminator, with the reflection diameter increasing with decreasing droplet contact angle, as in the top left illustration. Insets present zoom[Ins from opposing ends of the substrate to help visualize the differences in diameters of the reflected light. The scale bars are 2 mm. The white arrow points from the tallest to the shortest droplets, which θ 0 ounterintuitively θ 0 orrespond to the narrowest to widest reflection diameters. ii) The plots show the droplet heights for droplets along the diagonal indicated by the white arrow for each of the arrays. The droplet heights were calculated from the reflection diameters. Data points and error bars are the mean and standard deviation, respectively, as determined for droplets within the same row along the diagonal (up to 7 drops per row for d = 1000 m, 28 for d = 250 m, and 38 for d = 50 m).

the reflection diameters according to Equation (S1) in the Sup porting Information, derived from geometric considerations (see Section S2.4, Supporting Information). This shows that it is indeed possible to create gradients using acceleration to dedip posting for 2D arrays of droplets from 1000 m and down to 50 m. However, the employed method of hand-dipping (Figure S7, Supporting Information) does not allow for quan titatively correlating dip to a ting parameters with droplet sizes. Still, we see that it is consistently possible to tune the droplet heights at least a factor of 3, which thereby puts a lower limit

of the accessible range of droplet heights. With an automated experimental setup, it would be possible to conduct a systematic optimization and likely be able to extend this range by tuning the experimental conditions, such as withdrawal acceleration.

3. Discussion

For droplet arrays featuring gradients in volumes to be practill cally useful, it is typically important that there is an appreciable

2. Cramber 2011 (1997) 2012 (1997) 2012 (1997) 2012 (1997) 2013 (1

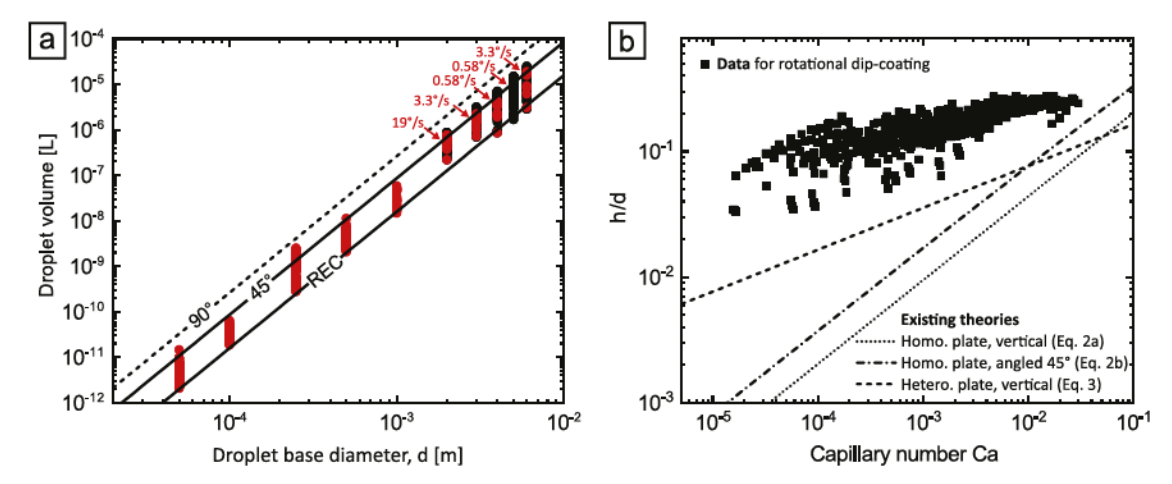


Figure 4. Production of gradient arrays at different length scales. a) Summary of the droplet volumes achieved for different droplet base diameters. The red data points exemplify volume variation achieved for a select angular speed (i.e., for the angular speed that gave the largest (relative) droplet variation in the array), while the black data points show the full range of demonstrated droplet volumes by including data from all investigated speeds. The conversion from experimentally measured heights to volume is obtained from ref. [28]. The theoretical diameter olume relationships for three different droplet contact angles (90 , 45 , and REC = 9 , the receding contact angle in the hydrophilic region) are denoted in the plot as three parallel lines. b) Experimentally measured height, h, for millimeter of h is included by rotational dip to a for vertical and angled (45) withdrawal.

size difference between the smallest and largest droplets within an array formed on a single substrate. The variation in droplet size achievable for a given substrate patterned with a single droplet footprint was assessed experimentally (Section 3.1) and compared to analytical theory (Section 3.2).

3.1. Summarizing Effect across Length Scales

Figure 4a shows the spread in droplet volumes for different biphilic substrates, each with a distinct hydrophilic spot dialmeter, which is indicated on the xaxis. The yaxis consists of the droplet volumes, obtained from the measured droplet heights using a spherical cap assumption, $V = \frac{\pi h}{6} \left(\frac{3}{4} d^2 + h^2 \right)$ where d is the droplet base diameter and h is its height. Each vertical cluster of points corresponds to data from a single biphilic substrate. Within each cluster, red dots correspond to volume variations across an array withdrawn with dipart ating parameters at the angular velocity that gave the highest spread in droplet volumes for that substrate. Meanwhile, the black dots are additional volumes achieved at other angular velocities for the same substrate, in order to show the full range of droplet volumes achieved for all withdrawal experiments in this study.

To indicate the wide range of droplet contact angles, θ , obtained, the theoretical relationship between droplet diam teter and volume $(V = \frac{\pi}{3}(2 + \cos\theta)(1 - \cos\theta)^2(\frac{d}{2\sin\theta})^3)$, derived from ref. [28] assuming negligible gravity) is plotted for three different droplet contact angles (90 , 45 , and REC = 9 , the receding contact angle in the hydrophilic region). We observed that the ability to vary volumes via acceleration mode dip to at the ability to vary volumes via acceleration of dip to a the droplet base diameter is decreased, which means that the method likely also works for both smaller and larger footprints than the 50 m to 6 mm range we have tested. This is important because the ability to create gradient arrays in a

parallel manner becomes increasingly more important as drop□ lets are scaled down, due to difficulties creating the droplets via other techniques (such as inkjet printing, [29] even when acousto□ phoretic printing is employed[30]) and the large number of drop□ lets makes it timeଢonsuming to produce them drop□byଢdrop.

3.2. Explaining Droplet Size with Analytical Theory

To rationalize the experimental data, and to understand the large spectrum of drop sizes that can be accessed on a single substrate, we applied wellkno wn theories for the thickness of the liquid layer entrained by a solid substrate withdrawn from a liquid bath. [31[39] Most studies have been conducted with unstructured, chemically homogenous substrates, where the film thickness scales as $h \sim \text{Ca}^{2/3}$. Here, $\text{Ca} = \frac{\mu u}{\sigma}$ is the capillary number, which characterizes the relative magnitude of viscous and surface tension forces; σ is the surface tension of the liquid and μ is the liquid viscosity. Also importantly, Krechetnikov and Homsy showed, by looking at the effect of roughness on the drag flow, that for small roughness features $(r/h \ll 1)$, the 2/3 thickness dependence is preserved. [40]

Landau, Levich, and Deryagin were the first to calculate the thickness of a film entrained on an infinite flat plate withdrawn vertically at the speed u from a reservoir. [31,32] Assuming that gravitational drainage is negligible and that the coating thick ness on a homogenous surface is established by a balance between viscous and capillary forces, they found

$$h = 0.946 \ell_c \text{Ca}^{2/3}$$
 (2a)

where Ca \ll 1 and $\ell_c = \left(\frac{\sigma}{\rho g}\right)^{\frac{1}{2}}$ is the capillary length; ρ is the

liquid density and g is the acceleration due to gravity. For a homogenous plate dragged out of a liquid reservoir at an angle α , Wilson^[35] showed that the film thickness is given by

www.advancedsciencenews.com



www.advmatinterfaces.de

$$h = \ell_{c} \operatorname{Ca}^{\frac{1}{2}} \frac{1}{(1 - \sin \alpha)^{\frac{1}{2}}} \left(0.946 \operatorname{Ca}^{\frac{1}{6}} - \frac{0.107 \cos \alpha}{1 - \sin \alpha} \operatorname{Ca}^{\frac{1}{2}} + \cdots \right)$$
 (2b)

For patterned surfaces, with wetting areas surrounded by nonwetting regions, experiments have demonstrated that the thickness h of the entrained fin is signifia ntly different from that on homogenous surfaces, due to the lateral confinement of the liquid which is not accounted for in Equations (2a) and (2b). [9] For vertically oriented hydrophilic strips of width d, Darhuber et al. [9] and Davis [41] showed that the fin thickness scales as

$$h = KdCa^{1/3}$$
 (3)

where K is a geometry \square ependent numerical constant (K = 0.356 for vertical withdrawal). From this scaling relation \square ship, we see that the droplet height is expected to increase with viscosity and decrease with surface tension, which is note \square worthy as researchers transition to applications using solvents other than water, or where solutes may decrease the surface tension.

We observe reasonable qualitative agreement between our rotational dipco ating experiments and the capillary number dependence in Equation (3) (Figure 4b; see Figure S6 in the Supporting Information for the determination of withdrawal speed, which was based on the timela pse imaging presented in Figure 2a). However, it is important to emphasize that the rotational motion, with its orthogonal velocity component, is expected to further increase the film thickness relative to both Equations (2) and (3), explaining the quantitative discrepancy between experiments and the theoretical analysis. Further more, Darhuber et al. found that hydrophilic regions interact to increase entrained volume when their separation is smaller than the capillary length.^[9] When applying Equation (3) to our experiments on hydrophilic circles, it is important to note that the \mathbf{fm} thickness h is a function of the capillary number Ca, and hence the characteristic extraction speed u. Because the distance x to the hinge varies across the sample, the withdrawal speed $u \sim \omega x^2$, where ω is the frequency of rotation, also dif fers. This allows us to vary the fm thickness across the sample because the local capillary numbers differ. Thus, our experi□ ments complement constants peed fm deposition on chemi□ cally patterned substrates (e.g., Brasjen et al. [6]) by substantially expanding the range of accessible film thicknesses on each substrate.

3.3. Future Opportunities

Gradient droplet array characteristics that can be tuned using these methods are the minimum and maximum droplet heights, the steepness of the gradient, and the monotonicity in the droplet height. Here, we studied the possibility to design these aspects by varying the linear and angular velocities of the substrate. Multiple other opportunities to tune the gradient exist, such as hydrophilic island distribution on the substrate. The distribution matters as neighboring spots distort the local reservoir meniscus, which in turn affects the sizes of entrained droplets. Neighboring droplets, orthogonal to the withdrawal direction, interact to increase entrained droplet sizes if their

separation is smaller than the capillary length (for water ≈2.7 mm). [9] For neighbors along the withdrawal direction, they can interact if meniscus deformation relaxation time is com□ parable to or longer than the period between their formations. Likewise, the meniscus is typically deformed at the edge of the substrate being withdrawn; the distance to the substrate edge needed to neglect edge effects is one capillary length or larger. Finally, it may also be possible to tune the gradient characteris□ tics by altering the evaporation dynamics, such as through vari□ ations in the geometrical configuration (e.g., using a smaller reservoir such that the substrate edges are close to the reservoir edges, affecting the meniscus) or environment (e.g., humidity, temperature) of the dipEb ating setup, as has been demon□ strated in the formation of films with gradients in thickness. [42]

While dipto ating of our biphilic substrate led to droplet array formation for all investigated speeds, it presumably does not happen for all speeds. For chemically homogenous par□ tially wetting substrates (i.e., also both our hydrophilic and hydrophobic regions when considered separately), there is a wettability dependent critical speed above which forced wetting sets in and results in film formation upon diptroating; below this critical speed the liquid reservoir simply recedes from the substrate, leaving it dry. [43] The consequence for biphilic sub□ strates is a functional range of withdrawal speeds within which a film forms in the hydrophilic regions (defines the minimum speed) while none forms in the hydrophobic ones (defines the maximum speed). However, our ability to predict this func□ tional range is limited as existing theories focus on structur. ally smooth and chemically homogenous substrates.[44[36] In fact, roughness affects the critical speed $^{[47,48]}$ and our chemical pattern distorts the triple line, which likely also leads to devia□ tion from existing models. Future experiments and models describing the critical speed as a function of surface roughness and chemical heterogeneity are essential to predicting min□ imum and maximum heights of withdrawn droplets. In turn, this will improve opportunities to tailor the array gradients to specific applications.

A potential drawback of dipEd ating, in general, is the large reservoir volume needed. Fortunately, since only the liquid near the reservoir surface is involved in droplet formation, one way to mitigate this may be to support the deposition liquid above an immiscible liquid (a Idlummy phase I), [49] especially useful if the deposition liquid is expensive, rare, or timeEv olving, e.g., highPu rity products or biological materials. For subImillimeter samples with reservoir sizes small enough for capillary forces to dominate gravity, we also envision that the reservoir could be supported midair via capillary forces.

Finally, by combining multiple gradients, combinatorial chemistry assays can be more readily performed. [50CB2] One way to achieve this is to use a two[3tep deposition method similar to the multistep method employed by Faustini et al. to create a continuous functionality gradient. [11] In this process, a 2D array with a 1D gradient (similar to those of Figure 3b) can be formed by acceleration [50] de dip [50] ating in a reservoir containing a substance A. The solvent is then allowed to evaporate in order to translate the volume gradient to a gradient in surface concen [53] This procedure is repeated with another substance B, with the substrate rotated 90 to its original orientation so that the second gradient is orthogonal to the first. Another approach



www.advancedsciencenews.com

MATERIALS INTERFACES

www.advmatinterfaces.de

4. Conclusion

Using rotational and linear dipcb ating setups in acceleration□ mode, we unlocked fast formation of gradient droplet arrays with footprints ranging from millimeters to micrometers. Rota□ tional dipEb ating was used for 1D arrays of millimeterslized droplets, while linear acceleration dipto ating was used for 2D arrays of micrometerslized droplets. We created gradients using droplets with base diameters from as large as 6 mm and down to 50 m, demonstrating that the method is applicable to droplet volumes spanning more than six orders of mag□ nitude. Within an array, droplet volumes spanned a factor of 3 to 9 depending on the droplet base diameter. The ability to tune the droplet volume is expected to continue at even shorter length scales as the effect showed no sign of diminishing for smaller base diameters, a valuable possibility as the droplets become increasingly more challenging and timeEb nsuming to produce using other methods when scaled down. The experi□ mentally measured volumedependence of the droplets on the withdrawal speed exhibits a similar powerla w dependence as expected from theoretical considerations of chemically heterog□ enous substrates. However, the absolute sizes of our droplets were larger than predicted, the exact cause for which remains unknown. The technique is easily compatible with digital droplet array sandwiching, which enables the fast formation of 2D combinatorial chemistry arrays. For the future, we envision combining reconfi urable substrates with acceleration no de dip@oating to increase versatility even further.

5. Experimental Section

In brief, the biphilic substrates were fabricated from 4" Si wafers via fi st employing a selfImasking RIE, with a mixture of sulfur hexafluoride and oxygen gases,^[15] (Pegasus DIRIE, STS, U.K.) to create nanoroughness followed by a photolithographic process (Figure S1 in the Supporting Information shows mask designs). A monolayer of FDTS was then selflassembled in a molecular vapor deposition system (MVD 100, MST, USA) followed by an acetone liftlbff process (see Section S1.1 in the Supporting Information for details). Wettability was characterized using the deflation droplet method as the liquid withdrawal properties were determined for the droplet retention (Attension Theta Optical Tensiometer equipped with a highlspeed camera (Motion Xtra N3 with Navitar, IDT)).[57] The liquid used was 18.2 MΩ MilliQ. For the millimeter [] sized droplets, a rotational dipleoater built from LEGO MINDSTORMS was used (Section S2.1 and Figures S2 and S3, Supporting Information) and droplet sizes were characterized with a Nikon D5600 camera using a disassembled computer monitor for the backlight. For the micrometer [] sized droplets, the withdrawal was performed by hand (Figure S7, Supporting Information) and characterized by taking top view images with a reflected light microscope (Zeiss Axio Zoom.V16, Zeiss, Germany) (Section S2.4, Supporting Information). For the 100 and 50 m droplets,

the substrates were positioned on a dry[lce[lchilled copper plate within 2 s after dipping to prevent signifi ant evaporation[Induced volume changes. Additional experimental details can be found in the Supporting Information.

Statistical Analysis: Figure 1a \square ii, contact angle measurements were performed with n=3. Figure 1a \square iii, SEM micrograph was analyzed manually in Image]. Figure 3a, each rotational speed was repeated fi e times and side \square iew images analyzed using custom \square ivritten scripts in MATLAB 2017b; outliers were preserved despite their cause being known as edge effects from the substrate. Same software was applied to analyze top \square ivew images in Figure 3b with custom \square ivritten scripts. Data were visualized and fi ted in Origin pro 2021.

Supporting Information

Supporting Information is available from the Wiley Online Library or from the author.

Acknowledgements

The fianc ial support from the Danish National Research Foundation (DNRF122), Villum Foundation (grant no. 9301) for Intelligent Drug Delivery and Sensing Using Microcontainers and Nanomechanics (IDUN), and the Novo Nordisk Foundation (NNF17OC0026910) II Microstructures, microbiota and oral delivery (MIMIO) is acknowledged. J.A. and A.V.S. were supported by Harvard University Materials Research Science and Engineering Center (MRSEC) under Award No. DMRID 2011754. N.K.M. was supported by an Excellence Ph.D. Scholarship from DTU Health Tech. Dr. Michael Aizenberg is thanked for his comments, and valuable inputs from Rajendra Prasad Shukla, Inhat Chyshankou, Anjali Achazhiyath Edathil, Aakil Lalwani, and En Te Hwu are acknowledged.

Confl ct of Interest

The authors declare no conflict of interest.

Data Availability Statement

The data that support the fid ings of this study are available from the corresponding author upon reasonable request.

Keywords

biphilic surfaces, combinatorial chemistry, droplet microarray technology, high@throughput screening, parallelization of experiments

Received: March 24, 2022 Revised: May 6, 2022 Published online: July 6, 2022

- [1] E. Ueda, P. A. Levkin, Adv. Mater. 2013, 25, 1234.
- [2] W. Feng, E. Ueda, P. A. Levkin, Adv. Mater. 2018, 30, 1706111.
- [3] N. K. Mandsberg, Adv. Mater. Interfaces 2021, 8, 2100815.
- [5] W. Lei, K. Demir, J. Overhage, M. Grunze, T. Schwartz, P. A. Levkin, Adv. Biosyst. 2020, 4, 2000073.

739,2022,22,Downloaded from https://onlinelibrary.wiley.com/doi/10.1002/admi.202200667, Wiley Online Library on [07/11/2022]. See the Terms and Conditions (https://onlinelibrary.wiley.com/terms-and-conditions) on Wiley Online Library for rules of use; OA articles are governed by the applicable Creative Communication (https://onlinelibrary.wiley.com/terms-and-conditions) on Wiley Online Library for rules of use; OA articles are governed by the applicable Creative Communication (https://onlinelibrary.wiley.com/terms-and-conditions) on Wiley Online Library for rules of use; OA articles are governed by the applicable Creative Communication (https://onlinelibrary.wiley.com/terms-and-conditions) on Wiley Online Library for rules of use; OA articles are governed by the applicable Creative Communication (https://onlinelibrary.wiley.com/terms-and-conditions) on Wiley Online Library for rules of use; OA articles are governed by the applicable Creative Communication (https://onlinelibrary.wiley.com/terms-and-conditions) on Wiley Online Library for rules of use; OA articles are governed by the applicable Creative Communication (https://onlinelibrary.wiley.com/terms-and-conditions) on Wiley Online Library for rules of use; OA articles are governed by the applicable Creative Communication (https://onlinelibrary.wiley.com/terms-and-conditions) on Wiley Online Library for rules of use; OA articles are governed by the applicable Creative Communication (https://onlinelibrary.wiley.com/terms-and-conditions) on Wiley Online Library for rules of use; OA articles are governed by the applicable Creative Communication (https://onlinelibrary.wiley.com/terms-and-conditions) on Wiley Online Library for rules of use; OA articles are governed by the applicable Creative Communication (https://onlinelibrary.wiley.com/terms-and-conditions) on Wiley Online Library for rules of use; OA articles are governed by the applicable Creative Communication (https://onlinelibrary.wiley.com/terms-and-conditions) on Wiley Online Library for rules of use; O

www.advancedsciencenews.com

www.advmatinte

- [6] B. J. Brasjen, H. M. J. M. Wedershoven, A. W. van Cuijk, A. A. Darhuber, Chem. Eng. Sci. 2017, 158, 340.
- [7] B. J. Brasjen, A. W. van Cuijk, A. A. Darhuber, Chem. Eng. Process. 2011, 50, 565.
- [8] M. A. C. van Gestel, B. He, A. A. Darhuber, Chem. Eng. Sci. 2020, 227, 115832.
- [9] A. a. Darhuber, S. M. Troian, J. M. Davis, S. M. Miller, S. Wagner, J. Appl. Phys. 2000, 88, 5119.
- [10] N. K. Mandsberg, O. Hansen, R. Taboryski, Sci. Rep. 2017, 7, 12794.
- [11] M. Faustini, D. R. Ceratti, B. Louis, M. Boudot, P. A. Albouy, C. Boissiël e, D. Grosso, ACS Appl. Mater. Interfaces 2014, 6, 17102.
- [12] R. L. Davis, S. Jayaraman, P. M. Chaikin, R. A. Register, *Langmuir* 2014, 30, 5637.
- [13] H. A. Biebuyck, G. M. Whitesides, Langmuir 1994, 10, 2790.
- [14] A. De Ryck, D. Quarl J. Colloid Interface Sci. 1998, 203, 278.
- [15] L. Schneider, M. Laustsen, N. Mandsberg, R. Taboryski, Sci. Rep. 2016, 6, 21400.
- [16] J. J. Bikerman, J. Colloid Sci. 1950, 5, 349.
- [17] K. Kawasaki, J. Colloid Sci. 1960, 15, 402.
- [18] C. G. L. Fumridge, J. Colloid Sci. 1962, 17, 309.
- [19] N. K. Mandsberg, R. Taboryski, Surf. Topogr.: Metrol. Prop. 2017, 5, 024001
- [20] L. Feng, Y. Zhang, J. Xi, Y. Zhu, N. Wang, F. Xia, L. Jiang, Langmuir 2008, 24, 4114.
- [21] B. Bhushan, M. Nosonovsky, Philos. Trans. R. Soc., A 2010, 368, 4713.
- [22] Y. X. Zhuang, O. Hansen, T. Knieling, C. Wang, P. Rombach, W. Lang, W. Benecke, M. Kehlenbeck, J. Koblitz, J. Micromech. Microeng. 2006, 16, 2259.
- [23] N. J. Shirtcliffe, G. McHale, M. I. Newton, C. C. Perry, F. B. Pyatt, Appl. Phys. Lett. 2006, 89, 10.
- [24] D. E. McCoy, V. E. McCoy, N. K. Mandsberg, A. V. Shneidman, J. Aizenberg, R. O. Prum, D. Haig, Proc. R. Soc. B 2019, 286, 20190589.
- [25] J. M. Campbell, H. K. Christenson, ACS Appl. Mater. Interfaces 2018, 10, 16893.
- [26] C. Allain, D. Ausserre, F. Rondelez, J. Colloid Interface Sci. 1984, 107, 5.
- [27] I. Langmuir, V. J. Schaefer, J. Am. Chem. Soc. 1937, 59, 2400.
- [28] A. D. Polyanin, A. V Manzhirov, Mathematics for Engineers and Physicists, Chapman and Hall/CRC, London/Boca Raton, FL 2006.

- [30] D. Foresti, K. T. Kroll, R. Amissah, F. Sillani, K. A. Homan, D. Poulikakos, J. A. Lewis, Sci. Adv. 2018, 4, eaat1659.
- [31] B. Landau, L. Levich, Acta Physicochim. URSS 1942, 17, 42.
- [32] B. M. Deryagin, S. M. Levi, Film Coating Theory, Focal, New York, 1964.
- [33] D. A. White, J. A. Tallmadge, Chem. Eng. Sci. 1965, 20, 33.
- [34] C. Y. Lee, J. A. Tallmadge, AIChE J. 1972, 18, 1077.
- [35] S. D. R. Wilson, J. Eng. Math. 1982, 16, 209.
- [36] O. Rg lat, R. Labrie, P. A. Tanguy, J. Comput. Phys. 1993, 109, 238.
- [37] P. R. Schunk, A. J. Hurd, C. J. Brinker, in *Liquid Film Coating* (Eds: S. F. Kistler, P. M. Schweizer), Springer, Dordrecht 1997, pp. 673 1708.
- [38] D. Quel [] Annu. Rev. Fluid Mech. 1999, 31, 347.
- [39] S. J. Weinstein, K. J. Ruschak, Annu. Rev. Fluid Mech. 2004, 36, 29.
- [40] R. Krechetnikov, G. M. Homsy, Phys. Fluids 2005, 17, 102108.
- [41] J. M. Davis, Phys. Fluids 2005, 17, 038101.
- [42] E. Bindini, G. Naudin, M. Faustini, D. Grosso, C. Boissi

 e, J. Phys. Chem. C 2017, 121, 14572.
- [43] R. V. Sedev, J. G. Petrov, Colloids Surf. 1991, 53, 147.
- [44] T. Shing Chan, T. Gueudr I, J. H. Snoeijer, Phys. Fluids 2011, 23, 112103.
- [45] P. Gao, L. Li, J. J. Feng, H. Ding, X. Y. Lu, J. Fluid Mech. 2016, 791,
- [46] T. S. Chan, J. H. Snoeijer, J. Eggers, Phys. Fluids 2012, 24, 072104.
- [47] R. Golestanian, E. Raphall, Europhys. Lett. 2001, 55, 228.
- [48] J. Eggers, Phys. Rev. Lett. 2004, 93, 094502.
- [49] D. R. Ceratti, B. Louis, X. Paquez, M. Faustini, D. Grosso, Adv. Mater. 2015, 27, 4958.
- [50] A. Kulesa, J. Kehe, J. E. Hurtado, P. Tawde, P. C. Blainey, Proc. Natl. Acad. Sci. USA 2018, 115, 6685.
- [51] M. Benz, A. Asperger, M. Hamester, A. Welle, S. Heissler, P. A. Levkin, *Nat. Commun.* 2020, 11, 5391.
- [52] W. Lei, K. Demir, J. Overhage, M. Grunze, T. Schwartz, P. A. Levkin, Adv. Biosyst. 2020, 4, 2000073.
- [53] D. Qin, Y. Xia, B. Xu, H. Yang, C. Zhu, G. M. Whitesides, Adv. Mater. 1999, 11, 1433.
- [54] A. A. Popova, S. M. Schillo, K. Dernir, E. Ueda, A. Nesterov Mueller, P. A. Levkin, Adv. Mater. 2015, 27, 5217.
- [55] G. Jogia, T. Tronser, A. Popova, P. Levkin, Microarrays 2016, 5, 28.
- [56] A. A. Popova, T. Tronser, K. Demir, P. Haitz, K. Kuodyte, V. Starkuviene, P. Wajda, P. A. Levkin, Small 2019, 15, 1901299.
- [57] T. Huhtamkli, X. Tian, J. T. Korhonen, R. H. A. Ras, Nat. Protoc. 2018, 13, 1521.